

## A Papkovitch–Neuber-based numerical approach to cracks with contact in 3D

M. HINTERMÜLLER<sup>†</sup>

*Department of Mathematics, University of Graz, 8010 Graz, Austria and Chair in Applied Mathematics, University of Sussex, Brighton, BN1 9RF UK*

V. A. KOVTUNENKO

*Department of Mathematics, University of Graz, 8010 Graz, Austria and Lavrent'ev Institute of Hydrodynamics, 630090 Novosibirsk, Russia*

AND

K. KUNISCH

*Department of Mathematics, University of Graz, 8010 Graz, Austria*

[Received on 30 January 2007; accepted on 24 February 2009]

The mathematical model of a crack with non-penetration conditions is considered in the framework of 3D elasticity. The spatial crack problem is investigated with respect to its numerical realization in the context of constrained optimization. Specifically, for homogeneous isotropic solids with planar cracks, a Papkovitch–Neuber-based representation is adopted. It allows to employ a primal–dual active set strategy with an unconditional global and monotone convergence property. The iterates turn out to be primarily feasible. Illustrative numerical examples are presented.

*Keywords:* crack with non-penetration; constrained optimization problem; primal–dual active set algorithm; Papkovitch–Neuber representation; numerical calculation.

### 1. Motivation and introduction

In the framework of 3D elasticity theory, we consider a mathematical model of cracks constrained by non-penetration conditions, which allow the contact of opposite crack faces, but not their penetration. Properties of well-posedness for such problems were studied in terms of variational methods by [Khludnev & Sokolowski \(1999\)](#) and [Khludnev & Kovtunenکو \(2000\)](#). In the present paper, we investigate a numerical approach to the constrained crack problems. Our considerations focus on 3D homogeneous isotropic solids with planar cracks. For 3D aspects of fracture mechanics, we refer to the classic concepts as presented by [Cherepanov \(1979\)](#), [Geubelle & Rice \(1995\)](#) and [Morozov & Petrov \(2000\)](#) and to their numerical treatment by [Aliabadi & Rooke \(1992\)](#) and [Stavroulakis \(2001\)](#).

Before starting with a detailed description, let us present a few illustrative examples motivating, on one hand, the consideration of non-penetration conditions for a crack and, on the other hand, the need of a fully 3D formulation. With respect to the latter aspect, in the present context we point out that we cannot expect a physically meaningful decoupling of the model into independent planar states, in general. Further, the assumption of stress-free crack faces is not applicable due to the specific loading

<sup>†</sup>Email: michael.hintermueller@uni-graz.at

and the spatial nature of the problems under consideration. Indeed, contact of crack faces is possible and gives rise to a non-zero normal stress (the contact force) at the crack faces. In the following, we illustrate these facts by means of numerical examples.

We consider the following rectangular geometry of a solid with a crack in the unit cube  $\{0 < x_1 < 1, 0 < x_2 < 1, |x_3| < 0.5\}$ . The solid is clamped at  $x_1 = 1$  and it is loaded by a traction force applied uniformly at the marked part of the boundary; see Fig. 1(a). Assuming the condition of mutual non-penetration for vertical displacements (along the  $x_3$ -axis) between the opposite surfaces of the crack in the  $\{x_3 = 0\}$ -plane, we compute a numerical solution of the elasticity problem. We find a contact zone of the crack surfaces which is indicated in black in Fig. 1(b). Following the standard terminology adopted in constrained optimization, this zone is referred to as the ‘active set’. The components of displacements and stresses at both crack surfaces are depicted, respectively, in Fig. 2. This example clearly illustrates the known influence of the boundary at  $x_2 = 0$  and  $x_2 = 1$  that restricts the applicability of planar models.

In the following examples 2 and 3, we keep the above geometry of the solid with crack and change the loading only. The configuration of Example 2 is shown in Fig. 3(a). The solution of the corresponding elasticity problem is depicted in a componentwise fashion in Fig. 4. We can see in Fig. 3(b) that the active (contact) zone is split into two separate sets, which exhibit no symmetry. Hence, planar models cannot be applied here.

Note that, due to the symmetry of the solid and the loading with respect to the  $\{x_3 = 0\}$ -plane, these two examples have zero jumps of tangential displacements across the crack (see the 1- and 2-components of  $\mathbf{u}$  in Figs 2 and 4) and a non-negative jump (opening) of the vertical displacement (i.e. the 3-component in Figs 2 and 4), thus implying a mode-1 state of the crack.

The last example illustrated in Fig. 5(a) deals with the case of the absence of a symmetry with respect to the  $\{x_3 = 0\}$ -plane. As a consequence, in Fig. 6 we can clearly see the appearance of a mixed state of mode-1, mode-2 and mode-3 of the crack, i.e. non-zero jumps for all displacement components across the crack. The active (contact) set forms an axis-symmetric region with respect to the  $\{x_2 = 0.5, x_3 = 0\}$ -axis in Fig. 5(b).

In the classical fracture mechanics context, one of the most intriguing aspects is to determine the stress intensity factors in three spatial dimensions. For its various theoretical and numerical concepts, we refer to [Nikishkov & Atluri \(1987\)](#), [Kachanov & Karapetian \(1997\)](#) and [Gosz \*et al.\* \(1998\)](#). The stress intensity factors  $(K_1, K_2, K_3)$  will help us to compare the obtained numerical results with the ones derived for the linearized model assuming stress-free crack faces. For this reason we adopt an

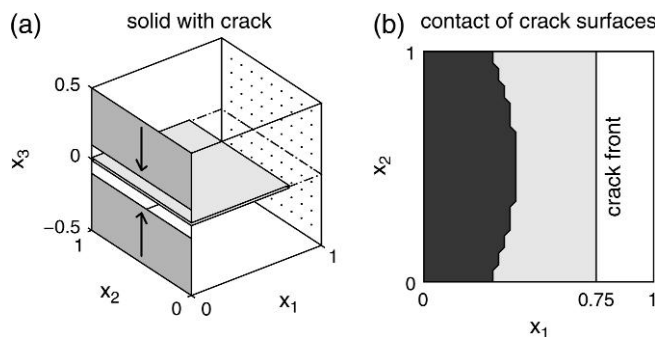


FIG. 1. Example 1: geometry and loading in the crack problem.

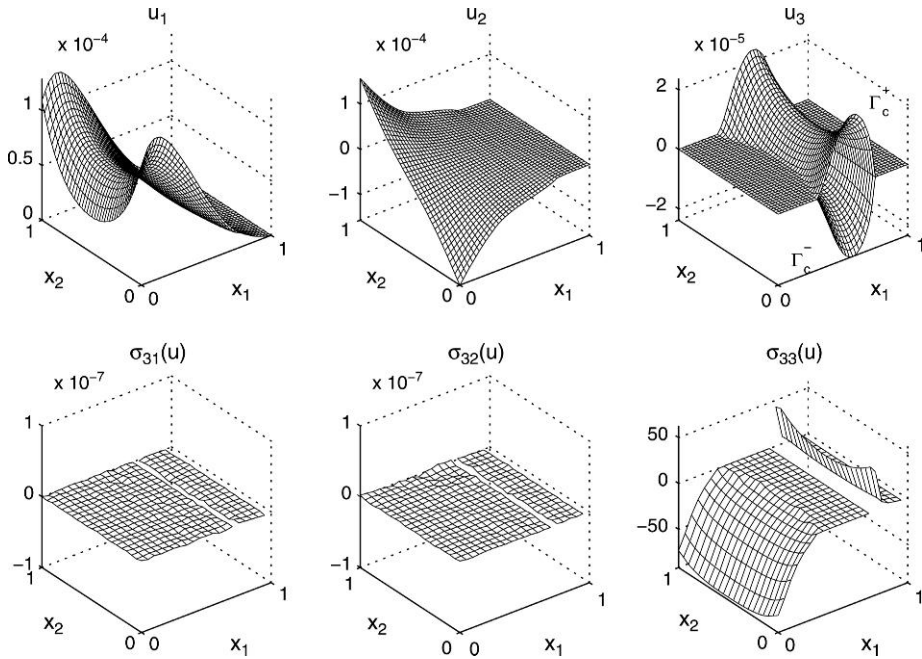


FIG. 2. Example 1: displacement and stress at the crack.

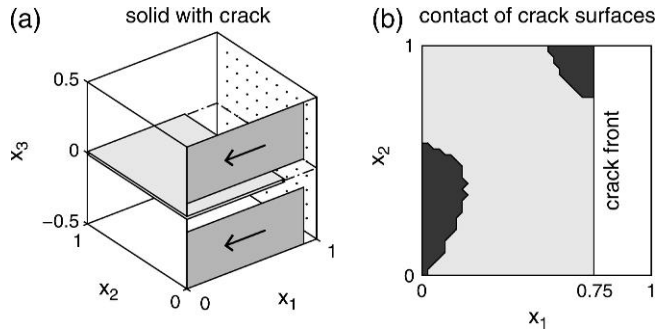


FIG. 3. Example 2: geometry and loading in the crack problem.

approximate formula, see [Cisilino & Aliabadi \(1999\)](#), which is useful in engineering practice:

$$(K_1, K_2, K_3) = \frac{E}{4(1-\nu^2)} \sqrt{\frac{\pi}{2h}} (\llbracket u_3^h \rrbracket, \llbracket u_1^h \rrbracket, (1-\nu)\llbracket u_2^h \rrbracket). \quad (1.1)$$

The jumps  $(\llbracket u_1^h \rrbracket, \llbracket u_2^h \rrbracket, \llbracket u_3^h \rrbracket)$  of the displacement components are evaluated at a distance  $h$  behind the crack front. The material parameters  $E$  and  $\nu$  stand for the Young's modulus and the Poisson ratio.

When the loading is chosen such that it prevents self-penetration of crack faces, validation of our numerical tools was given in [Kovtunenکو \(2006b\)](#). The results were compared with an exact 3D solution which obeys the known square-root singularities. The example configuration of the present paper forces

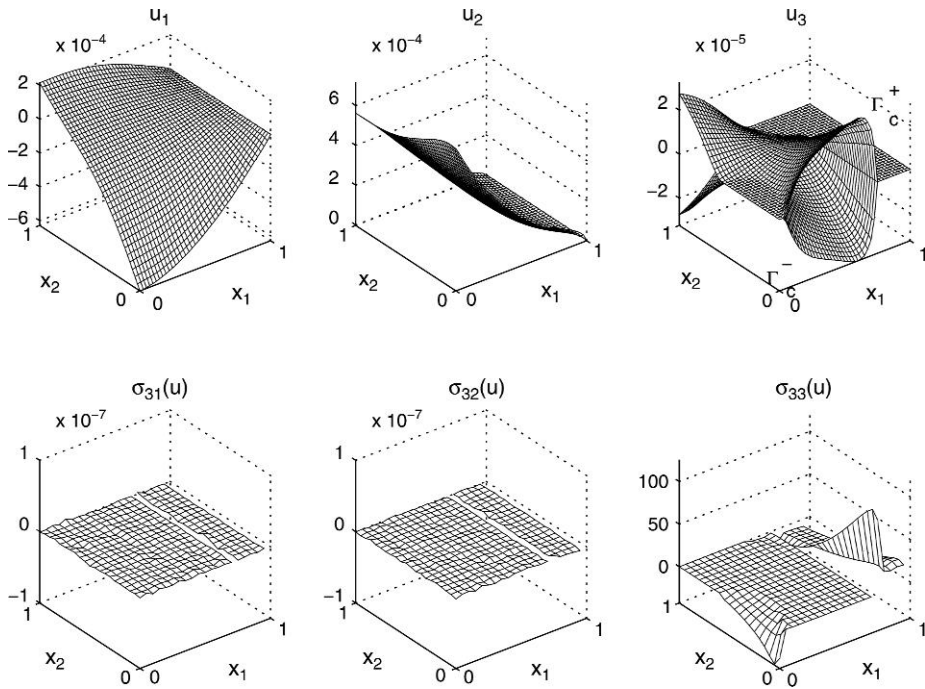


FIG. 4. Example 2: displacement and stress at the crack.

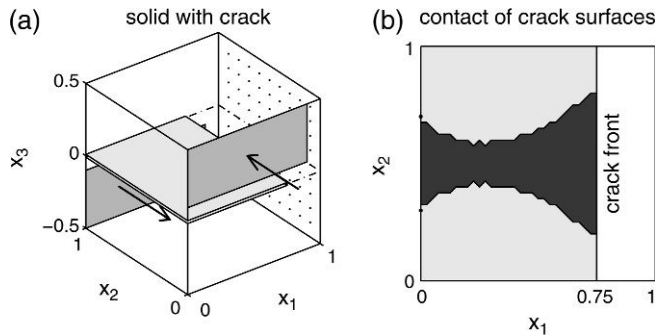


FIG. 5. Example 3: geometry and loading in the crack problem.

contact between the crack faces. As a consequence, the difference between models occurs when we take into account non-penetration conditions or ignore them in the model.

First, the result of numerical calculation of the stress intensity factors by formula (1.1) is depicted in Fig. 7 for the geometry and the loading given in Examples 1 and 2. Since  $[[u_1^h]] = 0$  and  $[[u_2^h]] = 0$  along the crack front, then  $K_2 = K_3 = 0$  in these examples. Hence, only the non-zero  $K_1$  is shown. In Fig. 7(a),  $K_1$  is calculated for the constrained crack model which prevents self-penetration. Respectively, in Fig. 7(b)  $K_1$  is given for the linearized model admitting penetration of the crack faces. The negative stress intensity factor  $K_1$  in Fig. 7(b) implies self-penetration of crack faces which is inconsistent

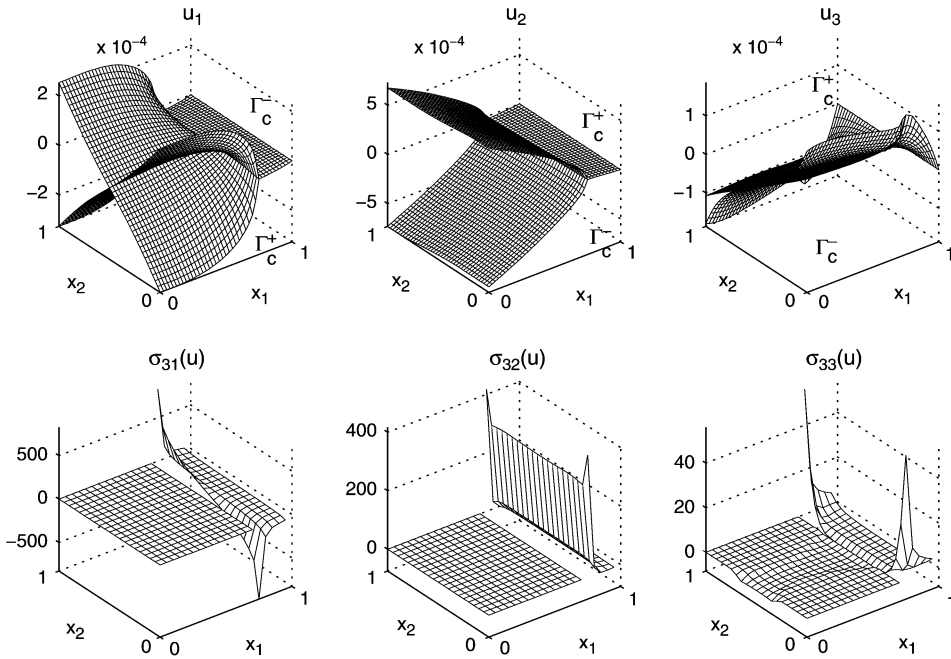


FIG. 6. Example 3: displacement and stress at the crack.

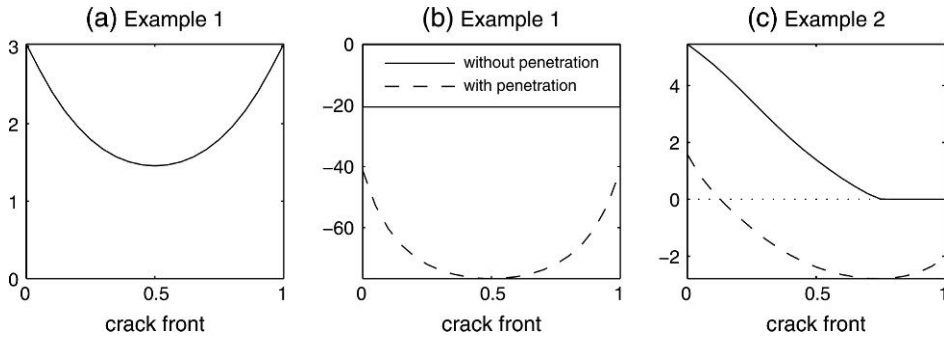


FIG. 7. The non-zero stress intensity factor  $K_1$  (MPa $\sqrt{m}$ ) at the crack front in Examples 1 and 2.

physically. It can be seen that due to the prescribed compression loading, the observed error of the linearized setting of the crack problem is tremendous in Example 1. The quantity  $K_1$  along the crack front in Example 2 is depicted in Fig. 7(c) for both models simultaneously. The dashed line corresponds to the model with penetration, whereas the solid line reflects the model without penetration. The figure shows the significant difference between the curves which implies that the assumption of stress-free crack faces is too coarse in this case.

Secondly, in the mixed-mode state of Example 3, all three stress intensity factors ( $K_1, K_2, K_3$ ) are non-zero, and they are depicted in Fig. 8. While two of them,  $K_2$  and  $K_3$ , visually coincide for the linearized and the constrained setting of the crack problem, the difference for  $K_1$  attains a relative error

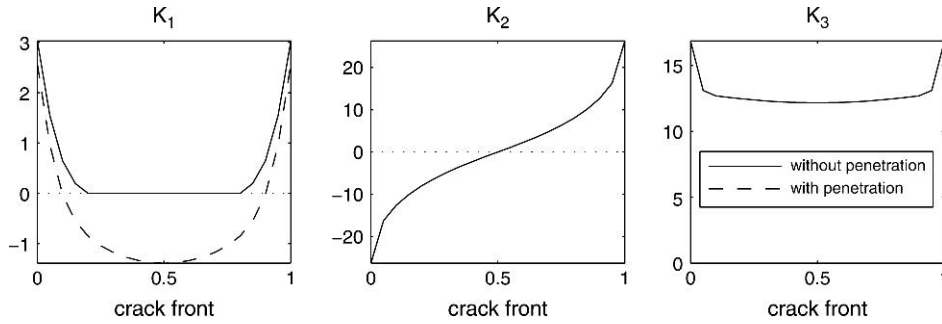


FIG. 8. The mixed-mode stress intensity factors  $K_1$ ,  $K_2$  and  $K_3$  ( $\text{MPa}\sqrt{\text{m}}$ ) at the crack front in Example 3.

of 47%. Even if we cut off the negative values of  $K_1$  at zero, an error of 21% remains for the linearized setting.

It is interesting to note that the difference of the stress intensity factors occurs only for  $K_1$  associated to the constrained component of the solution of the crack problem.

For computing a solution of crack problems with non-penetration conditions, we apply the so-called ‘primal–dual active set strategy’, which is based on a semi-smooth differentiability property of the operator of the problem (see, [Ito & Kunisch, 2003](#); [Hintermüller \*et al.\*, 2003](#)). It is a very efficient tool to solve constrained optimization problems. The reason lies in the fact that a primal state variable (displacement) and a dual state variable (normal stress) are used simultaneously to determine an active (contact) set properly, even in cases when the two variables are close to zero. Compared to, e.g. purely primal approaches which are based on  $\mathbf{u}$  only, our primal–dual technique is numerically more stable. In fact, it typically avoids possible chattering phenomena of the algorithm due to primal degeneracy, i.e. very flat transitions of the jump of the displacement across the crack into the active set. In the present paper, we investigate global convergence properties of this strategy based on a Papkovitch–Neuber representation in 3D elasticity.

From a general point of view, the principal difficulty of a convergence analysis of the primal–dual algorithm concerns here the absence of a maximum principle for vector-valued coupled systems. Therefore, we utilize asymptotic arguments based on a ‘Papkovitch–Neuber representation’ of the 3D Lamé equations via harmonic potentials, which obey the required maximum principle. Let us briefly recall the main formulas; see [Goldstein & Entov \(1994\)](#) for details. For the vector-valued Lamé equation in the space  $\{\mathbf{x} \in \mathbb{R}^3\}$ , e.g.

$$-\mu \Delta \mathbf{v} - (\mu + \lambda) \nabla (\text{div } \mathbf{v}) = \mathbf{f}, \quad (1.2)$$

the solution can be represented as

$$\mathbf{v} = \frac{1}{\mu} \boldsymbol{\psi} - \frac{\kappa}{2\mu} \nabla (\mathbf{x}^\top \boldsymbol{\psi} - \phi), \quad \kappa = \frac{\mu + \lambda}{2\mu + \lambda} \quad (1.3)$$

by the functions  $\boldsymbol{\psi} = (\psi_1, \psi_2, \psi_3)$  and  $\phi$  satisfying

$$-\Delta \boldsymbol{\psi} = \mathbf{f}, \quad -\Delta \phi = \mathbf{x}^\top \mathbf{f}. \quad (1.4)$$

Here  $\mu > 0$  and  $\lambda > 0$  denote the Lamé parameters and  $\mathbf{f}$  is a volume force. For  $\mathbf{f} = \mathbf{0}$  and with the particular choice

$$\psi_\alpha = \mu(\kappa - 1)U_\alpha \quad (\alpha = 1, 2), \quad \psi_3 = \mu(\kappa + 1)U_3, \quad \phi = \mu(\kappa - 1)\mathbf{x}^\top \mathbf{U}$$

in (1.4), where  $\mathbf{U}$  satisfies

$$\Delta \mathbf{U} = \mathbf{0}, \quad \operatorname{div} \mathbf{U} = 0 \quad (\text{e.g. } \mathbf{U} = \nabla \Phi, \Delta \Phi = 0), \quad (1.5)$$

the representation (1.3) reads as

$$v_\alpha = (\kappa - 1)U_\alpha - \kappa x_3 U_{3,\alpha} \quad (\alpha = 1, 2), \quad v_3 = U_3 - \kappa x_3 U_{3,3}. \quad (1.6)$$

The relations (1.6) imply a decoupling of the third components  $v_3$  of the variables from  $(v_1, v_2)$  at the  $\{x_3 = 0\}$ -plane:

$$v_3 = U_3, \quad \sigma_{33}(\mathbf{v}) := 2\mu v_{3,3} + \lambda \operatorname{div} \mathbf{v} = 2\mu\kappa U_{3,3} \quad \text{at } x_3 = 0. \quad (1.7)$$

As a consequence of (1.5) and (1.7), positivity/negativity properties of  $v_3$  and  $\sigma_{33}(\mathbf{v})$  are determined from the following Hopf (strong) maximum principle for the harmonic function  $U_3$ :

The derivative  $U_{3,3}$  (hence  $\sigma_{33}(\mathbf{v})$ ) is strictly negative/positive at the maximum/minimum of  $U_3$  (hence  $v_3$ ) at the boundary.

Employing these well-known constructions we are able to define a primal–dual active set strategy with an unconditional global and monotone convergence property in Section 2. Section 3 is devoted to computational features of our numerical algorithm for the examples presented at the beginning of this section.

We remark that a purely primal numerical method for constrained crack problems is presented in Zozulya & Menshykov (2003). For advanced discretization techniques, we refer to the meshless finite-element methods modelling 3D cracks as developed by Sukumar *et al.* (2000) and to the adaptive finite elements in contact problems by Hu *et al.* (2000).

## 2. Continuous setting of the problem

### 2.1 The mixed boundary-value formulation of a constrained crack problem

Let  $\Gamma_C$  be a planar crack posed on the plane  $\{x_3 = 0\}$  and located inside a domain  $\Omega \subset \mathbb{R}^3$  with the boundary  $\partial\Omega = \Gamma$ . The crack  $\Gamma_C$  is assumed to be an open set in the plane  $\{x_3 = 0\}$ . For the vector  $\mathbf{u} = (u_1, u_2, u_3)^\top(\mathbf{x})$  of displacements of a point  $\mathbf{x} = (x_1, x_2, x_3)^\top \in \mathbb{R}^3$ , we introduce the standard tensors of 3D elasticity for the stress and strain as

$$\begin{aligned} \sigma_{ij}(\mathbf{u}) &= 2\mu \varepsilon_{ij}(\mathbf{u}) + \lambda \delta_{ij} \operatorname{div} \mathbf{u}, \\ \varepsilon_{ij}(\mathbf{u}) &= 0.5(u_{i,j} + u_{j,i}) \quad (i, j = 1, 2, 3), \end{aligned} \quad (2.1)$$

with the Lamé parameters  $\mu$  and  $\lambda$ . For a given load  $\mathbf{f} = (f_1, f_2, f_3)^\top(\mathbf{x})$ , we consider the following problem of an equilibrium in  $\Omega_C = \Omega \setminus \Gamma_C$  of a solid with the crack subject to ‘non-penetration conditions’ written in the strong form:

$$-\mu \Delta \mathbf{u} - (\mu + \lambda) \nabla(\operatorname{div} \mathbf{u}) = \mathbf{f} \quad \text{in } \Omega_C, \quad (2.2a)$$

$$\mathbf{u} = \mathbf{0} \quad \text{on } \Gamma, \quad (2.2b)$$

$$\sigma_{13}(\mathbf{u}) = \sigma_{23}(\mathbf{u}) = 0 \quad \text{on } \Gamma_C^\pm, \quad (2.2c)$$

$$\llbracket u_3 \rrbracket \geq 0, \quad \sigma_{33}(\mathbf{u}) \leq 0, \quad \sigma_{33}(\mathbf{u}) \llbracket u_3 \rrbracket = 0 \quad \text{on } \Gamma_C, \quad (2.2d)$$

with the jump  $\llbracket u_3 \rrbracket = u_3|_{\Gamma_C^+} - u_3|_{\Gamma_C^-}$  across the crack surfaces  $\Gamma_C^\pm$ .

The weak formulation of (2.2) as a variational inequality, i.e.

$$\int_{\Omega_C} \sigma_{ij}(\mathbf{u}) \varepsilon_{ij}(\mathbf{v} - \mathbf{u}) dx \geq \int_{\Omega_C} f_i (v - u)_i ds \quad \text{for all } \mathbf{v} \in K,$$

where

$$K = \{\mathbf{v} \in H^1(\Omega_C)^3: \mathbf{v} = \mathbf{0} \text{ on } \Gamma, \llbracket v_3 \rrbracket \geq 0 \text{ on } \Gamma_C\},$$

provides us with the generalized solution  $\mathbf{u} \in K$  to (2.2). The solution satisfies the complementarity conditions (2.2d) in the weak form:

$$\llbracket u_3 \rrbracket \geq 0 \text{ on } \Gamma_C, \quad \langle \sigma_{33}(\mathbf{u}), \llbracket v_3 - u_3 \rrbracket \rangle_{\Gamma_C} \leq 0 \text{ for all } \mathbf{v} \in K.$$

The notation  $\langle \cdot, \cdot \rangle_{\Gamma_C}$  stands for the duality pairing between elements of the mutual dual spaces  $H^{1/2}$  and  $H^{-1/2}$  at  $\Gamma_C$ ; see [Khludnev & Kovtunenکو \(2000\)](#) for a detailed description of the dual spaces of traces at the crack. In the above reference, additional local  $H^2$ -regularity of the solution is established except at the crack front. As a consequence,  $\sigma_{33}(\mathbf{u}) \in H_{\text{loc}}^{1/2}(\Gamma_C)$ , i.e. for any  $\bar{\mathbf{x}} \in \Gamma_C$ ,  $\bar{\mathbf{x}} = (x_1, x_2)^\top$ , there exists a neighbourhood  $O(\bar{\mathbf{x}}) \subset \Gamma_C$  such that  $\sigma_{33}(\mathbf{u}) \in H^{1/2}(O(\bar{\mathbf{x}}))$ . In particular,  $\sigma_{33}(\mathbf{u})$  is almost everywhere well defined in  $\Gamma_C$ .

The complementarity condition (2.2d) can therefore be expressed equivalently as mixed boundary conditions, with equalities holding in the almost everywhere sense, as follows:

$$\llbracket u_3 \rrbracket = 0 \text{ on } A, \quad \sigma_{33}(\mathbf{u}) = 0 \text{ on } I := \Gamma_C \setminus A, \quad (2.3)$$

where the strongly ‘active set’  $A \subseteq \Gamma_C$  is defined by

$$A = \{\bar{\mathbf{x}} \in \Gamma_C: (c\sigma_{33}(\mathbf{u}) + \llbracket u_3 \rrbracket)(\bar{\mathbf{x}}, 0) < 0\}, \quad (2.4)$$

where  $c > 0$  is an arbitrary constant. The complementary ‘inactive set’  $I$  is given by

$$I = \{\bar{\mathbf{x}} \in \Gamma_C: (c\sigma_{33}(\mathbf{u}) + \llbracket u_3 \rrbracket)(\bar{\mathbf{x}}, 0) \geq 0\},$$

which also contains the weakly active set

$$\{\bar{\mathbf{x}} \in \Gamma_C: (c\sigma_{33}(\mathbf{u}) + \llbracket u_3 \rrbracket)(\bar{\mathbf{x}}, 0) = 0\}.$$

For properties of the equivalence between mixed formulations and variational inequalities, see [Kovtunenکو \(2006a\)](#).

In the following section, a primal–dual active set strategy suggested by the mixed formulation (2.3–2.4) will be analysed. At each iteration level  $n = -1, 0, \dots$ , a problem of the type (2.2a–2.2c) will be solved with the additional constraints that  $\llbracket u_3^{(n+1)} \rrbracket = 0$  on the currently strongly active set  $A^{(n)}$  and  $\sigma_{33}(\mathbf{u}^{(n+1)}) = 0$  on the complement of  $A^{(n)}$ . Such a procedure can be very efficient numerically. Its mathematical analysis is complicated by the fact that the solution of the intermediate problems  $\mathbf{u}^{(n+1)}$  can be less regular than the solution  $\mathbf{u}$  of the limit problem. In fact,  $\sigma_{33}(\mathbf{u}^{(n+1)})$  belongs to  $H_{\text{loc}}^{-1/2}(\Gamma_C)$  with singularities along the boundary of  $A^{(n)}$ . In the previous work, regularization by penalization or discretization was considered. After regularization, the primal–dual active set strategy, which is equivalent to a semi-smooth Newton method, is used. Its local convergence analysis follows from [Hintermüller](#)

*et al.* (2003) and Ito & Kunisch (2003). However, a monotone global convergence property is available only in specific cases; see Hintermüller *et al.* (2004) for examples.

In the present work, we investigate the primal–dual active set strategy without regularization. We shall require, instead, an assumption on the regularity of the active sets  $A^{(n)}$  of the intermediate problems, which will allow a pointwise almost every interpretation of  $\llbracket u_3^{(n+1)} \rrbracket$  and  $\sigma_{33}(\mathbf{u}^{(n+1)})$ . We shall further rely on a formulation of the constrained crack problem in  $\mathbb{R}^3$ -space by asymptotic arguments. Using the Papkovitch–Neuber representation for a solution of the mixed problem of linear elasticity in a half-space, we prove global and monotone convergence properties of the iterates of the primal–dual active set strategy in  $\mathbb{R}^3$ . This property is confirmed by our numerical findings in Section 3.

### 2.2 The primal–dual active set strategy in $\mathbb{R}^3$ -space

In this section, we neglect the influence of the external boundary  $\Gamma$  and consider the problem on all of  $\mathbb{R}^3$ . This relates to the situation where we concentrate on the behaviour of the system (2.2) in a neighbourhood of the crack. We investigate the following problem on  $\mathbb{R}^3 \setminus \Gamma_C$ :

$$\begin{aligned} -\mu \Delta \mathbf{u} - (\mu + \lambda) \nabla(\operatorname{div} \mathbf{u}) &= \mathbf{f} \quad \text{in } \mathbb{R}^3 \setminus \Gamma_C, \\ \mathbf{u}(\mathbf{x}) &= \mathbf{o}(1) \quad \text{as } |\mathbf{x}| \rightarrow \infty, \\ \sigma_{13}(\mathbf{u}) = \sigma_{23}(\mathbf{u}) &= 0 \quad \text{on } \Gamma_C^\pm, \\ \llbracket u_3 \rrbracket \geq 0, \quad \sigma_{33}(\mathbf{u}) \leq 0, \quad \sigma_{33}(\mathbf{u}) \llbracket u_3 \rrbracket &= 0 \quad \text{on } \Gamma_C. \end{aligned} \tag{2.5}$$

Since  $\sigma_{33}(\mathbf{u})$  has a pointwise almost everywhere meaning in the open set  $\Gamma_C$ , the complementarity condition in (2.5), i.e. the last three relations, can be stated as mixed boundary conditions with respect to the active set  $A$  and its inactive complement  $I$  in  $\Gamma_C$ :

$$\begin{aligned} \llbracket u_3 \rrbracket &= 0 \quad \text{on } A = \{\bar{\mathbf{x}} \in \Gamma_C : (c\sigma_{33}(\mathbf{u}) + \llbracket u_3 \rrbracket)(\bar{\mathbf{x}}, 0) < 0\}, \\ \sigma_{33}(\mathbf{u}) &= 0 \quad \text{on } I := \Gamma_C \setminus A. \end{aligned}$$

We define a primal–dual active set algorithm corresponding to (2.5).

#### ALGORITHM 1

- (0) Choose  $A^{(-1)} \subset \mathbb{R}^2$ ; set  $n = -1$ .
- (1) Solve for  $\mathbf{u}^{(n+1)}$ :

$$\begin{aligned} -\mu \Delta \mathbf{u}^{(n+1)} - (\mu + \lambda) \nabla(\operatorname{div} \mathbf{u}^{(n+1)}) &= \mathbf{f} \quad \text{in } \mathbb{R}^3 \setminus \Gamma_C, \\ \mathbf{u}^{(n+1)}(\mathbf{x}) &= \mathbf{o}(1) \quad \text{as } |\mathbf{x}| \rightarrow \infty, \\ \sigma_{13}(\mathbf{u}^{(n+1)}) = \sigma_{23}(\mathbf{u}^{(n+1)}) &= 0 \quad \text{on } \Gamma_C^\pm, \\ \llbracket u_3^{(n+1)} \rrbracket(\bar{\mathbf{x}}, 0) &= 0 \quad \text{for } \bar{\mathbf{x}} \in A^{(n)}, \\ \sigma_{33}(\mathbf{u}^{(n+1)})(\bar{\mathbf{x}}, 0) &= 0 \quad \text{for } \bar{\mathbf{x}} \in I^{(n)} := \Gamma_C \setminus A^{(n)}. \end{aligned} \tag{2.6}$$

(2) Compute the active set:

$$A^{(n+1)} = \{\bar{\mathbf{x}} \in \Gamma_C: (c\sigma_{33}(\mathbf{u}^{(n+1)}) + \llbracket u_3^{(n+1)} \rrbracket)(\bar{\mathbf{x}}, 0) < 0\}. \quad (2.7)$$

(3) If  $A^{(n+1)} = A^{(n)}$  then STOP; else set  $n = n + 1$  and go to Step 1.

In the following, we rely on the assumption which guarantees that the iterates  $\sigma_{33}(\mathbf{u}^{(n+1)})$  are defined almost everywhere in  $\Gamma_C$ . This, in turn, will be implied by an assumption that at each iteration level the interface between strongly active  $A^{(n)}$  and inactive  $I^{(n)}$  sets is sufficiently regular so that  $\sigma_{33}(\mathbf{u}^{(n+1)}) \in H_{\text{loc}}^{1/2}(A^{(n)})$ .

LEMMA 2.1 For all  $n = -1, 0, \dots$ , we assume that  $A^{(n)} = \bigcup_{i=0}^{\infty} A_i^{(n)}$ , where  $A_i^{(n)} = \overset{\circ}{A}_i^{(n)} \subset \mathbb{R}^2$  are pairwise disjoint sets of  $\text{meas}(A_i^{(n)}) \neq 0$  for  $i = 1, \dots, \infty$  and  $\text{meas}(A_0^{(n)}) = 0$  in  $\mathbb{R}^2$ . If the respective boundaries of  $A_i^{(n)} \cap \Gamma_C$  are sufficiently smooth for  $i = 1, \dots, \infty$ , then the normal stress  $\sigma_{33}(\mathbf{u}^{(n+1)})$  is defined pointwise almost everywhere at  $\Gamma_C$ .

The assertion of Lemma 2.1 follows directly from standart results on the local smoothness of the solution to mixed boundary-value problems.

The stopping rule of Algorithm 1 is justified by the following considerations. If we assume that  $A^{(n)} = A^{(n+1)}$ , then from (2.7) we infer  $\sigma_{33}(\mathbf{u}^{(n+1)}) < 0$  at  $A^{(n+1)}$  and  $\llbracket u_3^{(n+1)} \rrbracket \geq 0$  at  $I^{(n+1)}$ . This, together with the conditions of (2.6) at  $\Gamma_C$ , proves that the iterates  $\mathbf{u}^{(n+1)}$  and  $A^{(n+1)}$  satisfy (2.5) if Algorithm 1 terminates in Step 3. In numerical experiments with properly chosen discretization, the algorithm typically terminates with  $A^{(n)} = A^{(n+1)}$ . If this was not the case, termination conditions based on residual must be used.

To investigate the behaviour of Algorithm 1, first we introduce the concept of feasibility. We call the iterate  $\mathbf{u}^{(n+1)}$  of (2.6) ‘feasible’ if  $\llbracket u_3^{(n+1)} \rrbracket \geq 0$  is satisfied at  $\Gamma_C$ . Second, we utilize a Papkovitch–Neuber representation of the Lamé operator with the help of harmonic functions, which allow us to rely on a Hopf maximum principle. It enables us to state feasibility and a resulting monotonicity property of the iteration process.

LEMMA 2.2 If an iterate  $\mathbf{u}^{(n)}$  of (2.6) is feasible, then  $\mathbf{u}^{(n+1)}$  is feasible, too, and

$$\llbracket u_3^{(n+1)} \rrbracket \geq \llbracket u_3^{(n)} \rrbracket \quad \text{on } \Gamma_C, \quad (2.8a)$$

$$A^{(n+1)} \subseteq A^{(n)}. \quad (2.8b)$$

*Proof.* Let us denote by  $\bar{\mathbf{u}} = \mathbf{u}^{(n+1)} - \mathbf{u}^{(n)}$ . If  $\llbracket u_3^{(n)} \rrbracket \geq 0$  at  $\Gamma_C$ , then the definition of  $A^{(n)}$  according to (2.7) and the boundary conditions at  $\Gamma_C$  according to (2.6) imply that  $\llbracket \bar{u}_3 \rrbracket = 0$  at  $A^{(n)}$  and

$$p := \sigma_{33}(\bar{\mathbf{u}}) = -\sigma_{33}(\mathbf{u}^{(n)}) \leq 0 \quad \text{at } I^{(n)}.$$

The difference of iterates (2.6) for  $n + 1$  and  $n$  reads as

$$-\mu \Delta \bar{\mathbf{u}} - (\mu + \lambda) \nabla(\text{div } \bar{\mathbf{u}}) = \mathbf{0} \quad \text{in } \mathbb{R}^3 \setminus \Gamma_C,$$

$$\bar{\mathbf{u}}(\mathbf{x}) = \mathbf{o}(1) \quad \text{as } |\mathbf{x}| \rightarrow \infty,$$

$$\sigma_{13}(\bar{\mathbf{u}}) = \sigma_{23}(\bar{\mathbf{u}}) = 0 \quad \text{on } \Gamma_C^{\pm},$$

$$\begin{aligned} \llbracket \bar{u}_3 \rrbracket(\bar{\mathbf{x}}, 0) &= 0 \quad \text{for } \bar{\mathbf{x}} \in A^{(n)}, \\ \sigma_{33}(\bar{\mathbf{u}})(\bar{\mathbf{x}}, 0) &= p(\bar{\mathbf{x}}) \quad \text{for } \bar{\mathbf{x}} \in I^{(n)}. \end{aligned} \tag{2.9}$$

For  $\mathbf{x} \in \mathbb{R}_+^3 := \{(\bar{\mathbf{x}}, x_3) \in \mathbb{R}^3 : x_3 > 0\}$ , we determine the functions

$$\begin{aligned} v_\alpha(\mathbf{x}) &= \bar{u}_\alpha(\bar{\mathbf{x}}, x_3) + \bar{u}_\alpha(\bar{\mathbf{x}}, -x_3) \quad (\alpha = 1, 2), \\ v_3(\mathbf{x}) &= \bar{u}_3(\bar{\mathbf{x}}, x_3) - \bar{u}_3(\bar{\mathbf{x}}, -x_3), \end{aligned} \tag{2.10}$$

which satisfy the following relations at the boundary  $\{x_3 = 0\}$ :

$$v_3(\bar{\mathbf{x}}, 0) = \llbracket \bar{u}_3 \rrbracket(\bar{\mathbf{x}}, 0), \quad \sigma_{33}(\mathbf{v})(\bar{\mathbf{x}}, 0) = 2\sigma_{33}(\bar{\mathbf{u}})(\bar{\mathbf{x}}, 0) \quad \text{for } \bar{\mathbf{x}} \in \mathbb{R}^2. \tag{2.11}$$

With the help of (2.10) and (2.11), we can rewrite (2.9) for the function  $\mathbf{v} = (v_1, v_2, v_3)^\top$  in  $\mathbb{R}_+^3$  as

$$\begin{aligned} -\mu \Delta \mathbf{v} - (\mu + \lambda) \nabla(\operatorname{div} \mathbf{v}) &= \mathbf{0} \quad \text{in } \mathbb{R}_+^3, \\ \mathbf{v}(\mathbf{x}) &= o(1) \quad \text{as } |\mathbf{x}| \rightarrow \infty, \\ \sigma_{13}(\mathbf{v}) = \sigma_{23}(\mathbf{v}) &= 0 \quad \text{on } \{x_3 = 0\}, \\ v_3(\bar{\mathbf{x}}, 0) &= 0 \quad \text{for } \bar{\mathbf{x}} \in \mathbb{R}^2 \setminus I^{(n)}, \\ (2\mu v_{3,3} + \lambda \operatorname{div} \mathbf{v})(\bar{\mathbf{x}}, 0) &= 2p(\bar{\mathbf{x}}) \quad \text{for } \bar{\mathbf{x}} \in I^{(n)}, \end{aligned} \tag{2.12}$$

where we used (2.1). The known ‘Papkovitch–Neuber representation’ of the mixed boundary-value problem (2.12) in a half-space expresses  $\mathbf{v}$  in the form

$$\begin{aligned} v_\alpha &= (\kappa - 1)U_\alpha - \kappa x_3 U_{3,\alpha} \quad (\alpha = 1, 2), \\ v_3 &= U_3 - \kappa x_3 U_{3,3} \quad \left( \kappa = \frac{\mu + \lambda}{2\mu + \lambda} \right) \end{aligned} \tag{2.13}$$

by three harmonic potentials  $\mathbf{U} = (U_1, U_2, U_3)^\top(\mathbf{x})$  such that  $\Delta \mathbf{U} = \mathbf{0}$  and  $\operatorname{div} \mathbf{U} = 0$ . As  $x_3 = 0$  from (2.13), it follows that

$$v_3(\bar{\mathbf{x}}, 0) = U_3(\bar{\mathbf{x}}, 0), \quad (2\mu v_{3,3} + \lambda \operatorname{div} \mathbf{v})(\bar{\mathbf{x}}, 0) = 2\mu \kappa U_{3,3}(\bar{\mathbf{x}}, 0). \tag{2.14}$$

Thus, the harmonic function  $U_3$  satisfies the relations

$$\begin{aligned} \Delta U_3 &= 0 \quad \text{in } \mathbb{R}_+^3, \\ U_3(\mathbf{x}) &= o(1) \quad \text{as } |\mathbf{x}| \rightarrow \infty, \\ U_3(\bar{\mathbf{x}}, 0) &= 0 \quad \text{for } \bar{\mathbf{x}} \in \mathbb{R}^2 \setminus I^{(n)}, \\ U_{3,3}(\bar{\mathbf{x}}, 0) &= \frac{1}{\mu \kappa} p(\bar{\mathbf{x}}) \leq 0 \quad \text{for } \bar{\mathbf{x}} \in I^{(n)}; \end{aligned} \tag{2.15}$$

hence,  $U_3(\bar{\mathbf{x}}, 0) \geq 0$  for  $\bar{\mathbf{x}} \in \mathbb{R}^2$  due to the ‘Hopf maximum principle’. As a consequence of (2.11) and (2.14) we infer (2.8a). The feasibility of  $\mathbf{u}^{(n+1)}$  and (2.7) leads to the assertion (2.8b). The proof is completed.  $\square$

To attain the feasibility property, the initialization  $A^{(-1)} = \emptyset$  in Step 0 of Algorithm 1 is suitable, as we shall see in the following lemma.

LEMMA 2.3 For the iterate  $\mathbf{u}^{(0)}$  satisfying

$$\begin{aligned} -\mu \Delta \mathbf{u}^{(0)} - (\mu + \lambda) \nabla(\operatorname{div} \mathbf{u}^{(0)}) &= \mathbf{f} \quad \text{in } \mathbb{R}^3 \setminus \Gamma_C, \\ \mathbf{u}^{(0)}(\mathbf{x}) &= \mathbf{o}(1) \quad \text{as } |\mathbf{x}| \rightarrow \infty, \\ \sigma_{13}(\mathbf{u}^{(0)}) = \sigma_{23}(\mathbf{u}^{(0)}) = \sigma_{33}(\mathbf{u}^{(0)}) &= 0 \quad \text{on } \Gamma_C, \end{aligned} \tag{2.16}$$

the next iterate  $\mathbf{u}^{(1)}$  is feasible.

*Proof.* Denoting by  $\bar{\mathbf{u}} = \mathbf{u}^{(1)} - \mathbf{u}^{(0)}$  with  $\mathbf{u}^{(0)}$  from (2.16), we arrive at

$$\begin{aligned} A^{(0)} &= \{\bar{\mathbf{x}} \in \Gamma_C: \llbracket u_3^{(0)} \rrbracket(\bar{\mathbf{x}}, 0) < 0\}, \\ I^{(0)} &= \{\bar{\mathbf{x}} \in \Gamma_C: \llbracket u_3^{(0)} \rrbracket(\bar{\mathbf{x}}, 0) \geq 0\}. \end{aligned}$$

Hence,  $\llbracket \bar{u}_3 \rrbracket > 0$  at  $A^{(0)}$  and  $p := \sigma_{33}(\bar{\mathbf{u}}) = 0$  at  $I^{(0)}$ . Employing the representations (2.10) and (2.13) again, similarly to (2.15), we arrive at

$$\begin{aligned} \Delta U_3 &= 0 \quad \text{in } \mathbb{R}_+^3, \\ U_3(\mathbf{x}) &= o(1) \quad \text{as } |\mathbf{x}| \rightarrow \infty, \\ U_3(\bar{\mathbf{x}}, 0) &> 0 \quad \text{for } \bar{\mathbf{x}} \in \mathbb{R}^2 \setminus I^{(0)}, \\ U_{3,3}(\bar{\mathbf{x}}, 0) &= \frac{1}{\mu\kappa} p(\bar{\mathbf{x}}) = 0 \quad \text{for } \bar{\mathbf{x}} \in I^{(0)}. \end{aligned}$$

Utilizing the Hopf maximum principle and assuming that there exists  $\bar{\mathbf{x}}_0 \in I^{(0)}$  such that  $U_3(\bar{\mathbf{x}}_0, 0) < 0$  attains its minimum, we obtain a contradiction to the condition  $U_{3,3}(\bar{\mathbf{x}}_0, 0) = 0$ . Therefore,  $U_3(\bar{\mathbf{x}}, 0) \geq 0$  at  $I^{(0)}$ . Thus, from (2.11) and (2.14), we derive  $\llbracket u_3^{(1)} \rrbracket \geq \llbracket u_3^{(0)} \rrbracket \geq 0$  at  $I^{(0)}$  and  $\llbracket u_3^{(1)} \rrbracket = 0$  at  $A^{(0)}$ .  $\square$

Summarizing the results of Lemmas 2.2 and 2.3, we conclude with the following proposition on ‘global convergence’.

PROPOSITION 2.1 Starting with a feasible iterate  $\mathbf{u}^{(n)}$  ( $n \geq 0$ ), the iterates of Algorithm 1 are monotone, i.e.

$$0 \leq \llbracket u_3^{(n)} \rrbracket \leq \llbracket u_3^{(n+1)} \rrbracket \leq \dots \leq \llbracket u_3^* \rrbracket \quad \text{on } \Gamma_C, \tag{2.17a}$$

$$\Gamma_C \supseteq A^{(n)} \supseteq A^{(n+1)} \supseteq \dots \supseteq A^*, \tag{2.17b}$$

for  $\mathbf{u}^*$  and  $A^*$  satisfying (2.5).

*Proof.* For the arbitrary, feasible iterate  $\mathbf{u}^{(n)}$  with  $\llbracket u_3^{(n)} \rrbracket \geq 0$ , let us consider  $\bar{\mathbf{u}} = \mathbf{u}^* - \mathbf{u}^{(n)}$  with  $\mathbf{u}^*$  fulfilling (2.5). Using the relations (2.5), we derive  $\llbracket \bar{u}_3 \rrbracket(\bar{\mathbf{x}}, 0) \geq 0$  for  $\bar{\mathbf{x}} \in A^{(n)}$  and  $p(\bar{\mathbf{x}}) := \sigma_{33}(\bar{\mathbf{u}})(\bar{\mathbf{x}}, 0) \leq 0$  for  $\bar{\mathbf{x}} \in I^{(n)}$ . Therefore, the same arguments as used from (2.10) to (2.15) for  $\bar{\mathbf{u}}$  imply  $\llbracket \bar{u}_3 \rrbracket \geq 0$  and, thus, (2.17a). Moreover,

$$A^* \cap I^{(n)} \subseteq \{\bar{\mathbf{x}} \in \mathbb{R}^2: \llbracket u_3^* \rrbracket(\bar{\mathbf{x}}, 0) = 0, \llbracket u_3^{(n)} \rrbracket(\bar{\mathbf{x}}, 0) > 0\} = \emptyset;$$

otherwise,  $\llbracket \bar{u}_3 \rrbracket < 0$  would yield a contradiction. The latter fact provides us with the assertion (2.17b).  $\square$

### 3. Discretized problem and numerical examples

#### 3.1 The primal–dual active set strategy after discretization

Here we return to the situation where  $\Omega$  is a bounded domain and consider in the finite  $N$ -dimensional space the vector  $\mathbf{X} = (X_1, \dots, X_N)^\top \in \mathbb{R}^N$  of unknowns, assembling in an appropriate way components of the displacement vector  $(u_1(\mathbf{x}^m), u_2(\mathbf{x}^m), u_3(\mathbf{x}^m))^\top$  at grid points  $\mathbf{x}^m$  with  $m = (1, \dots, N/3)$  in the domain  $\Omega_C$  with a crack. We assume that a jump  $[[u_3]]$  across the crack  $\Gamma_C$  is described by differences  $u_3(\mathbf{x}^m) - u_3(\mathbf{x}^k)$  with  $\mathbf{x}^m \in \Gamma_C^+$  and  $\mathbf{x}^k \in \Gamma_C^-$ , thus forming a matrix  $\mathbf{A} \in \mathbb{R}^{|B| \times N}$  of a full column rank  $|B| < N$  for a set of indices  $B$ . We also suppose that the non-penetration condition reads  $\mathbf{A}\mathbf{X} \geq \mathbf{0}$ . Associated with a boundary traction  $\sigma_{33}(\mathbf{u})$  at  $\Gamma_C$ , an unknown vector  $\mathbf{Y} = (Y_1, \dots, Y_N)^\top \in \mathbb{R}^{|B|}$  stands for dual variables (a Lagrange multiplier). For  $\mathbf{F} \in \mathbb{R}^N$  given, after a suitable discretization of (2.2a–2.2c), (2.3) and (2.4) we arrive at the linear complementarity problem

$$\begin{aligned} \mathbf{L}\mathbf{X} + \mathbf{A}^\top \mathbf{Y} &= \mathbf{F}, \\ (\mathbf{A}\mathbf{X})_m &= 0 \quad \text{for all } m \in A = \{k \in B: (c\mathbf{Y} + \mathbf{A}\mathbf{X})_k < 0\}, \\ Y_m &= 0 \quad \text{for all } m \in I = \{k \in B: (c\mathbf{Y} + \mathbf{A}\mathbf{X})_k \geq 0\}, \end{aligned} \tag{3.1}$$

with the stiffness matrix  $\mathbf{L} \in \mathbb{R}^{N \times N}$  which is symmetric and positive definite.

Similar to Algorithm 1, a primal–dual active set strategy applied to (3.1) implies the following iteration.

#### ALGORITHM 2

- (0) Choose  $A^{(-1)} \subset B$ ; set  $n = -1$ .
- (1) Solve for  $(\mathbf{X}^{(n+1)}, \mathbf{Y}^{(n+1)}) \in \mathbb{R}^N \times \mathbb{R}^{|B|}$ :

$$\begin{aligned} \mathbf{L}\mathbf{X}^{(n+1)} + \mathbf{A}^\top \mathbf{Y}^{(n+1)} &= \mathbf{F}, \\ (\mathbf{A}\mathbf{X}^{(n+1)})_m &= 0 \quad \text{for all } m \in A^{(n)}, \\ Y_m^{(n+1)} &= 0 \quad \text{for all } m \in I^{(n)} := B \setminus A^{(n)}. \end{aligned} \tag{3.2}$$

- (2) Compute the active set:

$$A^{(n+1)} = \{k \in B: (c\mathbf{Y}^{(n+1)} + \mathbf{A}\mathbf{X}^{(n+1)})_k < 0\}. \tag{3.3}$$

- (3) If  $A^{(n+1)} = A^{(n)}$  then STOP; else set  $n = n + 1$  and go to Step 1.

In [Hintermüller et al. \(2004\)](#), the well-posedness of the linear problem (3.2) with fixed  $n$  was investigated in the general context of positive-definite matrices. Further, the locally superlinear convergence and sufficient conditions for a global convergence to the solution of (3.1) as  $n$  increases were given. Based on the unconditional results of Section 2, in the following we present in details computational features of Algorithm 2 applied to a homogeneous isotropic solid with a planar crack.

Note that Algorithm 2 is not immediately a discrete version of Algorithm 1. This is due to the fact that system (3.2) represents a discrete version of the elasticity problem with certain settings on  $A^{(n)}$  and  $I^{(n)}$  on the bounded domain  $\Omega_C$ . However, if the far-field influence is small, then the stiffness matrix  $\mathbf{L}$  is close to the discrete operator of the problem on the unbounded domain.

3.2 Geometric and physical data of the problem

Let us treat Example 2 from Section 1 as the basic example for this and the next sections. We consider the unite cube  $\Omega = \{0 < x_1 < 1, 0 < x_2 < 1, |x_3| < 0.5\}$  containing inside the crack  $\Gamma_C = \{0 < x_1 < 0.75, 0 < x_2 < 1, x_3 = 0\}$ . We assume that a volume load  $\mathbf{f} = \mathbf{0}$ , that the solid occupying the domain  $\Omega_C = \Omega \setminus \Gamma_C$  is clamped at  $\{x_1 = 1, 0 < x_2 < 1, |x_3| \leq 0.5\}$  and that it is loaded by a traction force at  $S = S^+ \cup S^-$ . The remain part of the boundary of  $\Omega$  is assumed to be stress free. The boundary loading is taken as

$$\begin{aligned}
 -\sigma_{12}(\mathbf{u}) &= -g, & -\sigma_{22}(\mathbf{u}) &= 0, & \sigma_{32}(\mathbf{u}) &= 0 \\
 \text{on } S^\pm &= \{0 < x_1 < 0.9, x_2 = 0, 0.1 < \pm x_3 < 0.5\}
 \end{aligned}
 \tag{3.4}$$

with the constant  $g = 0.001\mu$ , Lamé parameters  $\lambda = 2\nu\mu/(1 - 2\nu)$  and  $\mu = 0.5E/(1 + \nu)$ , where  $\nu = 0.34$  and  $E = 73000$  (MPa), thus  $g \approx 27$  (MPa). In Examples 1 and 3 of Section 1, instead of (3.4) we had

$$\begin{aligned}
 -\sigma_{13}(\mathbf{u}) &= \mp g, & -\sigma_{11}(\mathbf{u}) &= -\sigma_{12}(\mathbf{u}) = 0 \\
 \text{on } S^\pm &= \{x_1 = 0, 0 < x_2 < 1, 0.1 < \pm x_3 < 0.5\}
 \end{aligned}$$

TABLE 1 Number of unknowns  $N$  for mesh size  $h$

Mesh size $h$	0.05	0.025	0.01(6)
No. of unknowns $N$	29106	211806	692106

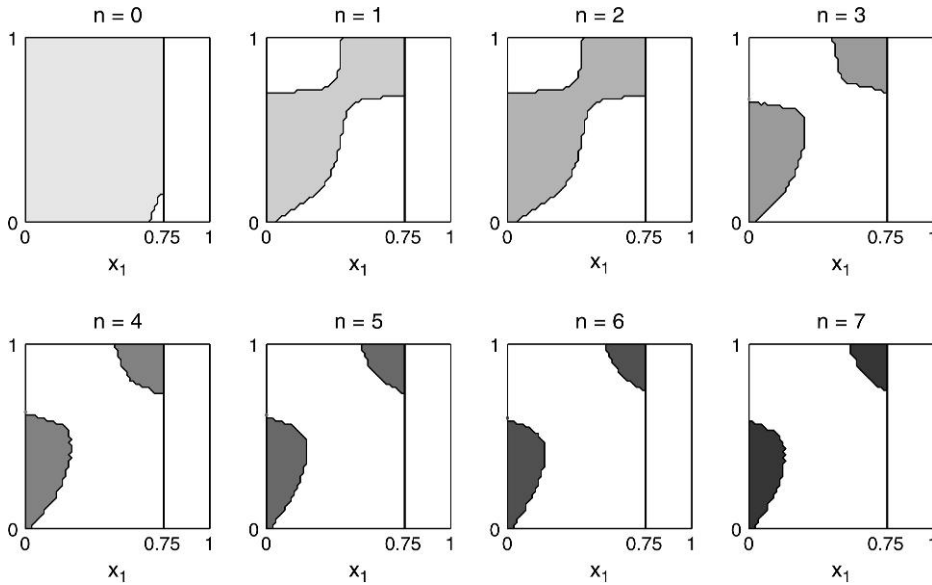


FIG. 9. Iterations  $A^{(n)}$  of the active set.

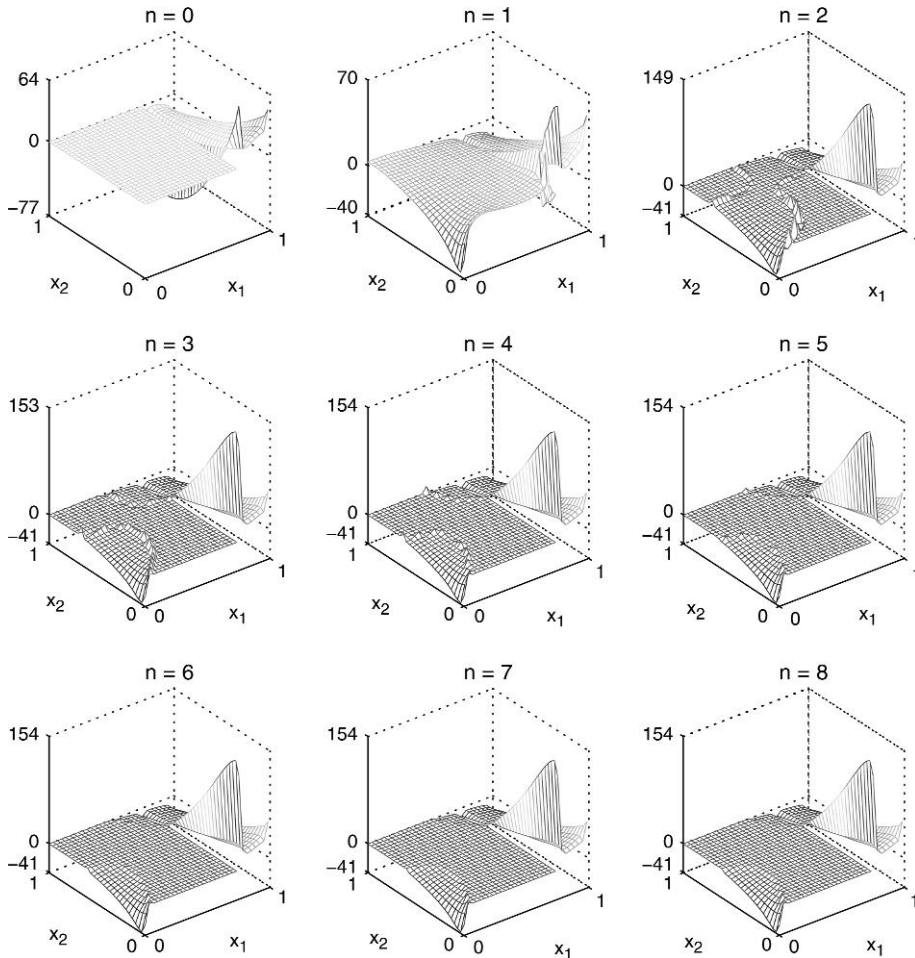


FIG. 10. Iterates  $\sigma_{33}(\mathbf{u}^{(n)})$  of the stress at  $\{x_3 = 0\}$ .

and

$$\begin{aligned}
 & -\sigma_{22}(\mathbf{u}) = \pm g, \quad -\sigma_{12}(\mathbf{u}) = -\sigma_{23}(\mathbf{u}) = 0 \\
 & \text{on } S^\pm = \{0 < x_1 < 0.9, x_2 = 0.5 \mp 0.5, 0.1 < \pm x_3 < 0.5\}.
 \end{aligned}$$

For the current feasibility study, we discretize the domain  $\Omega_C$  with a crack by a uniform triangulation and apply standard linear finite elements. Accounting double points located symmetrically at the interface with crack  $\{0 < x_1 < 1, 0 < x_2 < 1, x_3 = 0\}$ , the number  $N$  of unknowns of  $\mathbf{X}$  for the 3D elasticity problem (3.1) is presented in Table 1 in dependence of the mesh size  $h$ .

To solve the matrix equation (3.2), inner loop Symmetric Successive Over Relaxation-iterations are terminated with  $\text{tol} = 10^{-10}$ . For the determination of the active set in (3.3), a constant  $c$  is taken in the range of  $(10^{-3}, 10^{-2})$ . In the case when  $c\mathbf{Y}^{(n+1)} + \mathbf{A}\mathbf{X}^{(n+1)}$  is close to zero, for computational reasons

it can be helpful to use instead of (3.3)

$$A^{(n+1)} = \{k \in B: (cY^{(n+1)} + AX^{(n+1)})_k < -\delta\}$$

with small  $\delta > 0$ . In our examples we used  $\delta = 10^{-10}$ .

### 3.3 Convergence of the numerical algorithm

Now we present the results of our numerical computations obtained by Algorithm 2 when solving problem (3.1) with the data from Section 3.2. In the following,  $h$  is fixed as  $h = 0.01(6)$ .

Starting with  $A^{(-1)} = \emptyset$ , the history of iterates  $A^{(n)}$  of the active set as  $n = 0, \dots, 7$  is illustrated in Fig. 9. Algorithm 2 was terminated in Step 3 with the same active set structure  $A^{(n+1)} = A^{(n)}$  at iteration  $n = 7$  (i.e. after nine iterates), thus reaching the exact solution  $(X^*, Y^*, A^*) = (X^{(n)}, Y^{(n)}, A^{(n)})$  to the

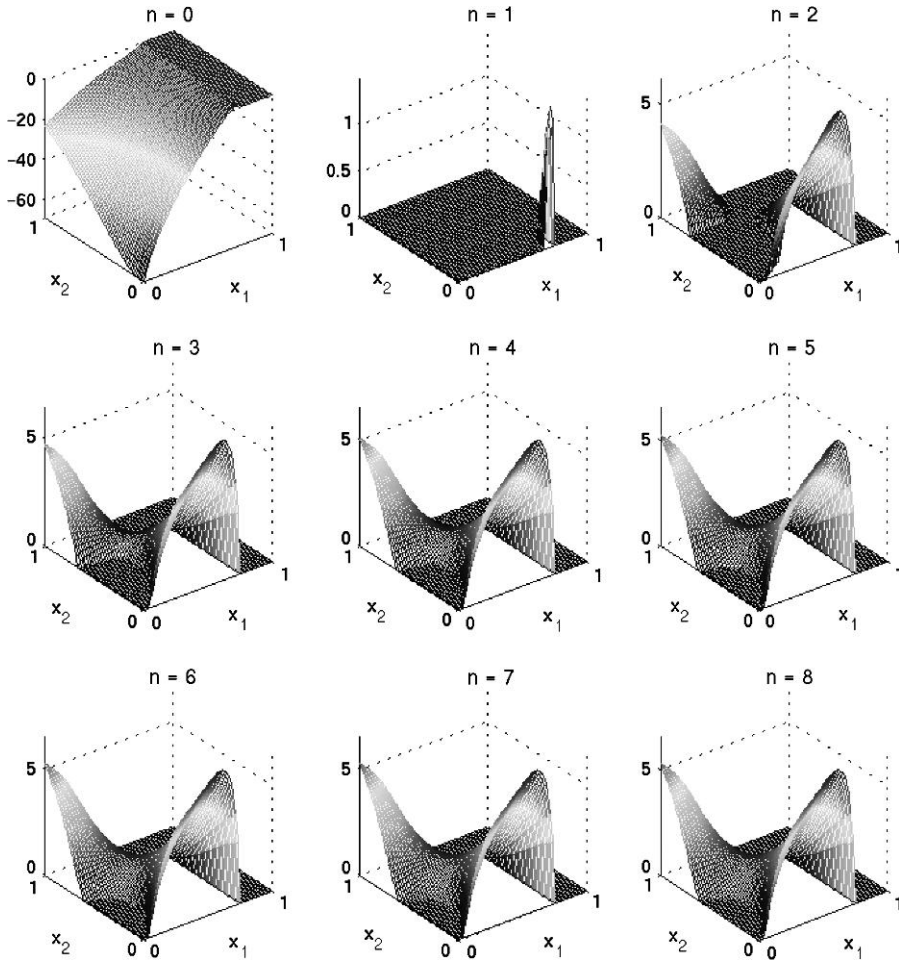


FIG. 11. Iterates  $\llbracket u_3^{(n)} \rrbracket \times 10^5$  of the jump at  $\{x_3 = 0\}$ .

discrete problem (3.1). During the iteration,  $A^{(0)}$  is split into two separate subsets. In Fig. 9, we observe monotone convergence of active sets:

$$\Gamma_C \supseteq A^{(1)} \supseteq \dots \supseteq A^{(n)} = A^{(n+1)} := A^*,$$

which is in accordance with Proposition 2.1.

The history of the iterates  $\llbracket u_3^{(n)} \rrbracket$  (respectively  $\mathcal{A}X^{(n)}$ ) of the jump of the displacements at the  $\{x_3 = 0\}$ -plane containing the crack  $\Gamma_C$  is depicted in Fig. 11. The corresponding stress  $\sigma_{33}(u^{(n)})$  reconstructed from the discrete Lagrange multiplier  $Y^{(n)}$  by means of a piecewise linear approximation is presented in Fig. 10.

Note that, for such initializations, problem (3.2) at  $n = 0$  represents an elasticity problem in the linear setting of stress-free crack surfaces without non-penetration conditions. Firstly, the corresponding active set  $A^{(0)}$  implies mutual interpenetration between the crack surfaces, as it can be viewed in Fig. 11, which is inconsistent physically. Secondly,  $A^{(0)}$  differs significantly from the true active set  $A^*$  depicted in the last plot of Fig. 9.

By refining the mesh, i.e. decreasing the mesh size  $h$ , the numerical solutions to (3.1) computed by Algorithm 2 for various  $h$  are compared with respect to the potential energy and the active set in Fig. 12(a,b), respectively. We observe linear convergence of the corresponding energies and that the active sets are close to each other.

The number of iterations required to successfully terminate Algorithm 2 is presented in Table 2. Note that it increases moderately with decreasing  $h$ .

The last two facts illustrate a stable behaviour of the primal–dual active set algorithm also with respect to the mesh refinement.

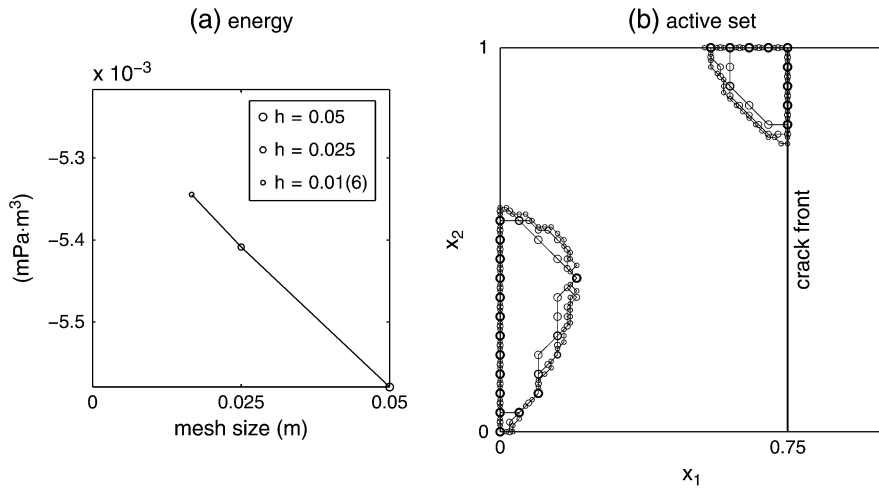


FIG. 12. Solution characteristics by decreasing  $h$ .

TABLE 2 *Number of iterations for mesh size  $h$*

Mesh size $h$	0.05	0.025	0.01(6)
No. of iterations	7	8	9

#### 4. Discussion

In this paper, a primal–dual active set strategy is proposed to numerically solve crack problems with non-penetration conditions. We focus on 3D aspects. On the basis of this approach, we present some of our findings in numerical experiments.

To interpret the physical implications we observe the following. The stress intensity factors  $K_2$  and  $K_3$  are not influenced significantly when frictionless contact occurs at the crack. On the contrary,  $K_1$  can take a negative value due to the contact implying self-penetration of crack faces. It happens often in the engineering practice that a small  $K_1 < 0$  can be ignored without essential loss of accuracy. However, we find that the error in  $K_1$  can be rather large in the following cases: First, it is evident that the pure compression loading gives rise to contact between the opposite crack faces. Secondly, for arbitrary loading applied at the boundary of a finite body the compression traction at a crack cannot be neglected in three spatial dimensions. In our examples, we demonstrate that boundary effects have a significant influence on the stress intensity factors. Thirdly, applying the commonly adopted simplification due to plane deformations disregards the 3D nature of contact at a crack.

#### Acknowledgement

We thank I.I. Argatov from St Petersburg for useful discussions on the mechanics.

#### Funding

Austrian Science Fund (FWF) in the framework of the START-program Y305 ‘Interfaces and Free Boundaries’, the research project P18267-N12 and the SFB F32 “Mathematical Optimization and Applications in Biomedical Sciences”; Russian Foundation for Basic Research (project 06-01-00209).

#### REFERENCES

- ALIABADI, M. H. & ROOKE, D. P. (1992) *Numerical Fracture Mechanics*. Southampton, UK: Kluwer.
- CHEREPANOV, G. P. (1979) *Mechanics of Brittle Fracture*. New York: McGraw-Hill.
- CISILINO, A. P. & ALIABADI, M. H. (1999) Three-dimensional boundary element analysis of fatigue crack growth in linear and non-linear fracture problems. *Eng. Fract. Mech.*, **63**, 713–733.
- GEUBELLE, P. H. & RICE, J. R. (1995) A spectral method for three-dimensional elastodynamic fracture problems. *J. Mech. Phys. Solids*, **43**, 1791–1824.
- GOLDSTEIN, R. V. & ENTOV, V. M. (1994) *Qualitative Methods in Continuum Mechanics*. Harlow, UK: Longman.
- GOSZ, M., DOLBOW, J. & MORAN, B. (1998) Domain integral formulation for stress intensity factor computation along curved three-dimensional interface cracks. *Int. J. Solids Struct.*, **35**, 1763–1783.
- HINTERMÜLLER, M., ITO, K. & KUNISCH, K. (2003) The primal-dual active set strategy as a semismooth Newton method. *SIAM J. Optim.*, **13**, 865–888.
- HINTERMÜLLER, M., KOVTUNENKO, V. A. & KUNISCH, K. (2004) The primal-dual active set method for a crack problem with non-penetration. *IMA J. Appl. Math.*, **69**, 1–26.
- HU, G.-D., PANAGIOTOPOULOS, P. D., PANAGOULI, O. K., SCHERF, O. & WRIGGERS, P. (2000) Adaptive finite element analysis of fractal interfaces in contact problems. *Comput. Methods Appl. Mech. Eng.*, **182**, 17–37.
- ITO, K. & KUNISCH, K. (2003) Semi-smooth Newton methods for the variational inequalities of the first kind. *ESAIM Math. Model. Numer. Anal.*, **37**, 41–62.
- KACHANOV, M. & KARAPETIAN, E. (1997) Three-dimensional interactions of a half-plane crack with point forces, dipoles and moments. *Int. J. Solids Struct.*, **34**, 4101–4125.

- KHLUDNEV, A. M. & KOVTUNENKO, V. A. (2000) *Analysis of Cracks in Solids*. Southampton, UK: WIT-Press.
- KHLUDNEV, A. M. & SOKOLOWSKI, J. (1999) The Griffith formula and the Rice–Cherepanov integral for crack problems with unilateral conditions in nonsmooth domains. *Eur. J. Appl. Math.*, **10**, 379–394.
- KOVTUNENKO, V. A. (2006a) Interface cracks in composite orthotropic materials and their delamination via global shape optimization. *Optim. Eng.*, **7**, 173–199.
- KOVTUNENKO, V. A. (2006b) Primal-dual sensitivity analysis of active sets for mixed boundary-value contact problems. *J. Eng. Math.*, **55**, 151–166.
- MOROZOV, N. F. & PETROV, YU. V. (2000) *Dynamics of Fracture*. Berlin: Springer.
- NIKISHKOV, G. P. & ATLURI, S. N. (1987) Calculation of fracture mechanics parameters for an arbitrary three-dimensional crack, by the ‘equivalent domain integral’ method. *Int. J. Numer. Methods Eng.*, **24**, 1801–1821.
- STAVROULAKIS, G. E. (2001) *Inverse and Crack Identification Problems in Engineering Mechanics*. Dordrecht, The Netherlands: Kluwer.
- SUKUMAR, N., MOËS, N., MORAN, B. & BELYTSCHKO, T. (2000) Extended finite element method for three-dimensional crack modelling. *Int. J. Numer. Math. Eng.*, **48**, 1549–1570.
- ZOZULYA, V. V. & MENSHYKOV, O. V. (2003) Use of the constrained optimization algorithms in some problems of fracture mechanics. *Optim. Eng.*, **4**, 365–384.